THE JOURNAL OF PHYSICAL CHEMISTRY Letters

Letter

pubs.acs.org/JPCL

The Reaction Mechanism and Capacity Degradation Model in Lithium Insertion Organic Cathodes, $Li_2C_6O_6$, Using Combined Experimental and First Principle Studies

Haegyeom Kim,[†] Dong-Hwa Seo,[†,#] Gabin Yoon,[†,⊥] William A. Goddard, III,[‡] Yun Sung Lee,*[,§] Won-Sub Yoon,*[,∥] and Kisuk Kang*[,†,⊥]

[†]Department of Materials Science and Engineering, Research Institute of Advanced Materials (RIAM), Seoul National University, Gwanak-ro 599, Gwanak-gu, Seoul 151-742, Republic of Korea

[‡]Materials and Process Simulation Center (MC 139-74), California Institute of Technology, 12000 East California Boulevard, Pasadena, California 91125, United States

[§]Faculty of Applied Chemical Engineering, Chonnam National University, Gwangju 500-757, Republic of Korea

[∥]Department of Energy Science, Sungkyunkwan University, Suwon 440-746, Republic of Korea

[⊥]Center for Nanoparticle Research, Institute for Basic Science (IBS), Seoul National University, Gwanak-ro 599, Gwanak-gu, Seoul 151-742, Republic of Korea

Supporting Information

ABSTRACT: Herein, we explore the capacity degradation of dilithium rhodizonate salt ($Li_2C_6O_6$) in lithium rechargeable batteries based on detailed investigations of the lithium de/insertion mechanism in $Li_2C_6O_6$ using both electrochemical and structural ex situ analyses combined with first-principles calculations. The experimental observations indicate that the $Li_xC_6O_6$ electrode undergoes multiple two-phase reactions in the composition range of $2 \leq x \leq 6$; however, the transformations in the range $2 \leq x \leq 4$ involve a major morphological change that eventually leads to particle exfoliation and the isolation of active material. Through first-principles analysis of $Li_xC_6O_6$ during de/lithiation, it was revealed that particle exfoliation is closely related to the crystal structural changes with lithium deinsertion from C_6O_6 interlayers of the $Li_xC_6O_6$. Among the lithium ions found at various sites, the extraction of lithium from C_6O_6 interlayers at $2 \leq x \leq 4$ decreases the binding force between the C_6O_6 layers, promoting the exfoliation of C_6O_6 layers and pulverization at the electrode, which degrades capacity retention.

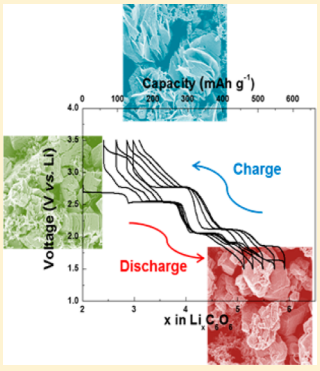

SECTION: Energy Conversion and Storage; Energy and Charge Transport

Lithium (Li)-ion batteries (LIBs) have been widely used as power sources for various applications due to their high energy and power densities.[1−8] In current LIB systems, inorganic materials that contain transition metals as redox elements are the most commonly used as cathodes. The high redox potential of the transition metals contributes to the high voltage, making high energy density LIBs possible.[2,5,9,10] However, to promote the sustainability of LIB manufacturing and to reduce the carbon footprint, shifting from inorganic to organic electrodes is important because electrodes based on organic materials can be synthesized from renewable resources such as biomass and can be prepared through eco-efficient processes.[11−15]

The concept of using organic materials as the electroactive components in LIBs is not new, as one of the first commercial LIBs employed a conducting polymer as the cathode material.[15,16] More recently, carbonyl compounds have been widely studied as cathodes, whereby the double bonds between carbon and oxygen (C═O) serve as the redox centers for Li storage.[14,15,17−20] In this series of materials, a high capacity can be achieved using a molecular design that maximizes the number of C═O redox centers per molecular weight. In this respect, dilithium rhodizonate salt ($Li_xC_6O_6$) was considered as an ideal candidate due to the high density of C═O groups available for Li storage.[14] The theoretical capacity of $Li_xC_6O_6$ ($2 \leq x \leq 6$) can be as high as 590 mAh g^{-1} with an average voltage of ∼2.4 V. Indeed, Chen et al. demonstrated that this system could deliver an energy density of 1100 Wh kg^{-1}, which is higher than that of conventional inorganic electrodes such as lithium cobalt oxide ($LiCoO_2$) and lithium iron phosphate ($LiFePO_4$; <600 Wh kg^{-1}).[14] Nevertheless, $Li_2C_6O_6$ electrodes exhibit a major drawback. This is the unacceptably poor cycle stability when applied as the electrode in conventional batteries. The substantial capacity degradation upon repeated cycling has hindered practical applications of $Li_2C_6O_6$, but the cause of this capacity degradation has not been established.

Received: July 24, 2014
Accepted: August 22, 2014
Published: August 22, 2014

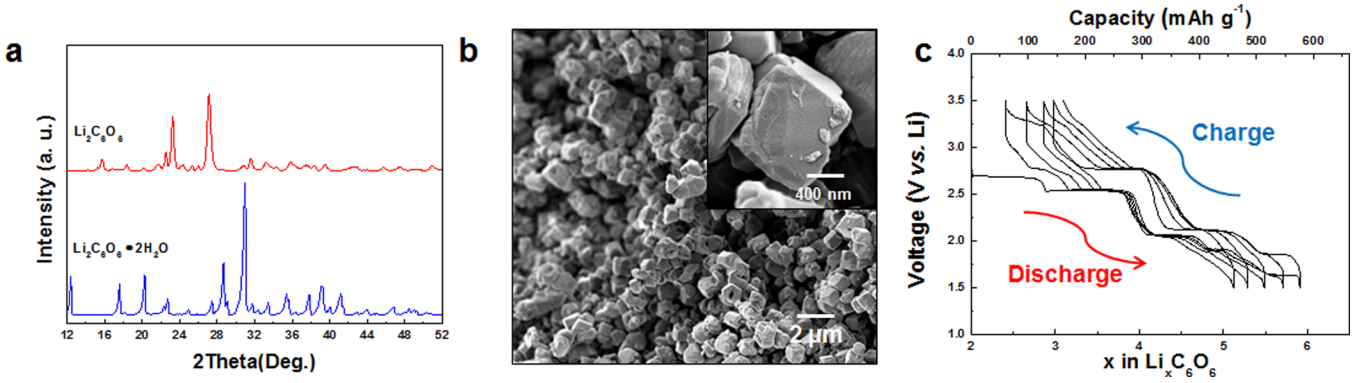

Figure 1. (a) XRD diffractograms of $Li_2C_6O_6 \cdot 2H_2O$ and $Li_2C_6O_6$. (b) An SEM image shows a $Li_2C_6O_6$ electrode. $Li_2C_6O_6$ was obtained by annealing $Li_2C_6O_6 \cdot 2H_2O$ at 200 °C to remove the waters of hydration. (c) The first five charge and discharge profiles of an as-synthesized $Li_2C_6O_6$ electrode are given from 1.5 to 3.5 V at 50 mA g^{-1}.

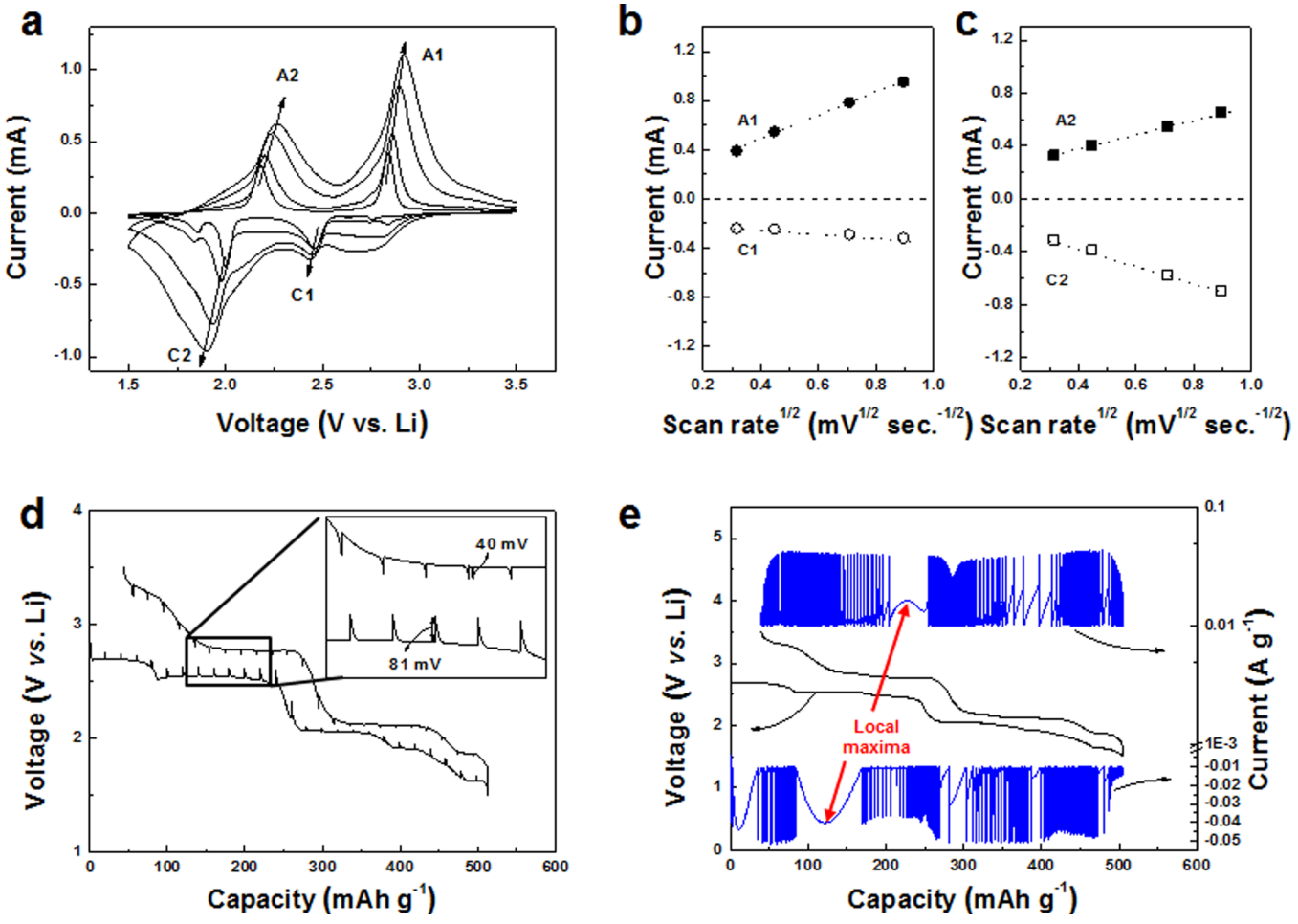

Figure 2. (a) CV analysis at various scan rates from 0.1 to 0.8 mV s^{-1}. The linear relationship between the square root of the scan rate and peak currents in (b) (A1 and C1) and (c) (A2 and C2) demonstrates that the de/lithiation reaction does not follow a surface limited process, but a diffusion-limited process. (d) Quasi-open-circuit potential (QOCP) measurements were performed at 20 mA g^{-1} with a 2-h relaxation time (dV/dt <10^{-5} V/s) for each charge and discharge. (e) Potentiostatic intermittent titration technique (PITT) measurements were performed on $Li_2C_6O_6$ electrodes using a "staircase" voltage profile whereby the cell potential was changed by 5 mV and the current was measured at each constant potential step as a function of time. Each individual titration was complete when the absolute current reached 10 mA g^{-1}. Blue line and black line indicate the current profile (vs capacity) and voltage plot (vs capacity), respectively.

In this study, we explored the cause of the capacity degradation of $Li_xC_6O_6$ ($2 \leq x \leq 6$) by investigating the details of the electrode reaction of $Li_xC_6O_6$ in the Li cell. Based on ex situ X-ray diffraction (XRD) and electrochemical analysis, we show that the $Li_xC_6O_6$ electrodes undergo multiple two-phase based transformations in the range of $2 \leq x \leq 6$. However, we find that the transformations occurring at $2 \leq x \leq 4$ involve a major microstructural change that leads to particle exfoliation. This observation is consistent with the electrochemical results showing that the capacity degrades much faster

dx.doi.org/10.1021/jz501557n | J. Phys. Chem. Lett. 2014, 5, 3086−3092

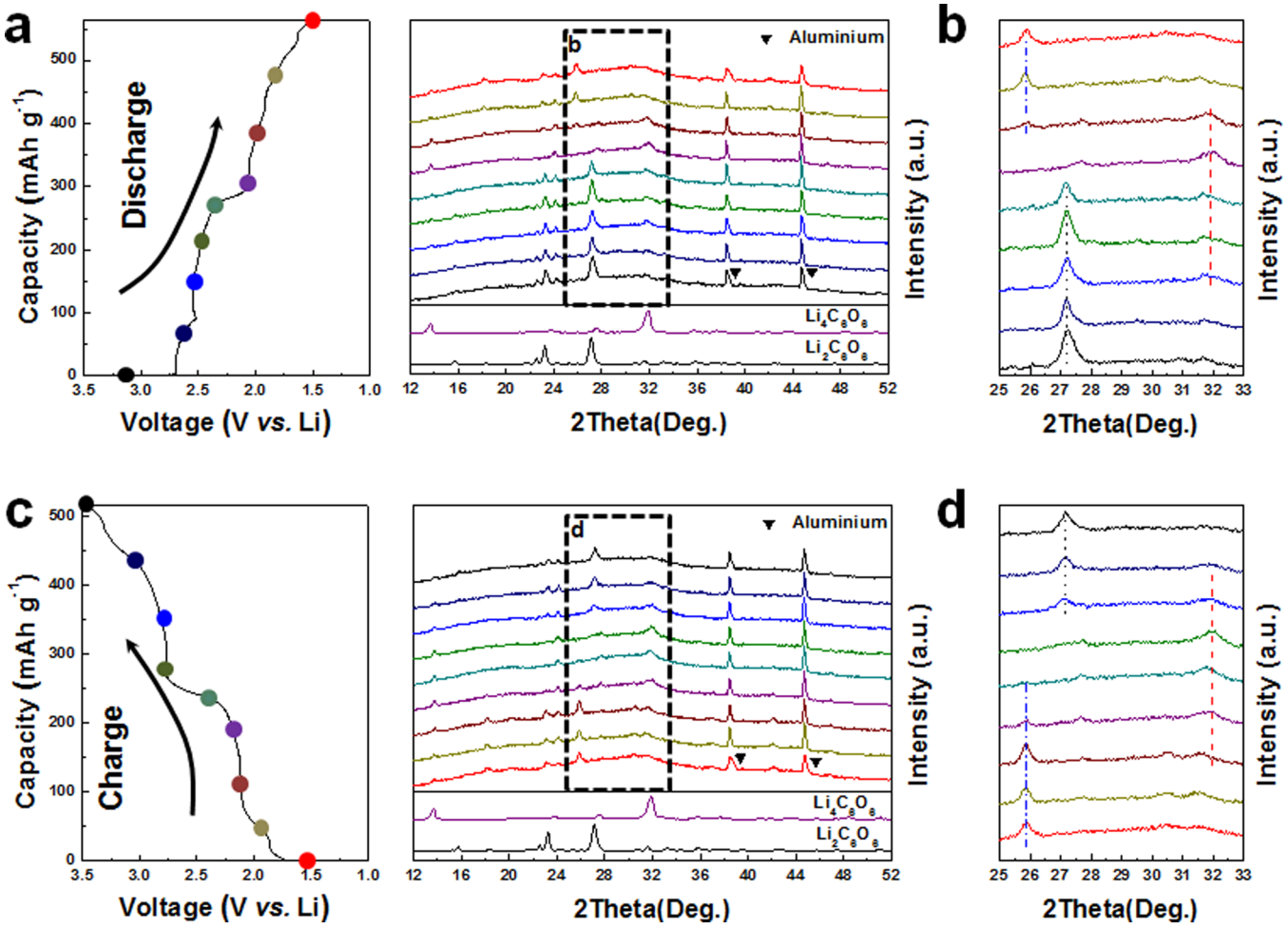

Figure 3. (a) A discharge profile of the $Li_2C_6O_6$ electrode is shown with ex situ XRD diffractograms obtained during the lithiation process; a magnified region of the diffractogram from 25° to 33° is given in (b). (c) A charge profile of the $Li_2C_6O_6$ electrode is shown with ex situ XRD diffractograms obtained during the delithiation process; a magnified region of the ex situ XRD diffractograms from 25° to 33° is presented in (d).

when the $Li_xC_6O_6$ electrode is cycled over this range. Although the capacity decay in most organic electrode materials has been mainly attributed to the dissolution of active material into the electrolyte,[18] our results suggest that the structural changes during cycling of organic electrodes must also be considered in order to enhance cycle stability.

A $Li_2C_6O_6$ sample was prepared by removing the crystal water from $Li_2C_6O_6{\cdot}2H_2O$ at 200 °C. XRD patterns of both $Li_2C_6O_6{\cdot}2H_2O$ and $Li_2C_6O_6$ in Figure 1a agree with those reported previously.[14] The TGA/DSC analysis in Figure S1 (Supporting Information) confirmed that the loss of water mainly occurred at ∼150−180 °C through an endothermic reaction, but $Li_2C_6O_6$ began to decompose above 250 °C through an exothermic reaction. The morphological study of as-synthesized $Li_2C_6O_6$ indicated that hexahedral-shaped particles with nearly monosizes of ∼800 nm were uniformly dispersed, as shown in Figure 1b. The electrochemical properties of the $Li_2C_6O_6$ electrodes were first examined using a galvanostatic charge/discharge experiment at a current rate of 50 mA g^{-1} between 1.5 and 3.5 V (Figure 1c). Upon discharge, distinctive plateaus became evident with an uptake of ∼4 Li ions to deliver a high specific capacity of ∼580 mAh g^{-1}, which agrees with the work of Chen et al.[14] When the electrode was charged, almost 4 Li ions were reversibly removed during the first cycle. However, the charge profile at $2 \leq x \leq 3$ became a sloping curve that differed from the discharge profile in the same region of the first cycle and decayed rapidly in subsequent cycles, which implied that some irreversible structural changes occurred during the charging process within this region. No further changes to the charge/discharge profile were observed in other regions. Cycling of $Li_2C_6O_6$ electrodes in various potential windows in Figure S2 also confirmed the limited reversibility of de/lithiation in the region of $2 \leq x \leq 4$. While a relatively small capacity degradation was observed for cycling between 1.5 and 2.4 V (84% retention after 30 cycles), significant capacity decay was evident for those between 2.2 and 3.5 V (37% retention after 30 cycles), demonstrating that capacity retention was significantly retarded by the electrochemical reaction between $Li_2C_6O_6$ and $Li_4C_6O_6$ in the higher voltage region (2.2 V−3.5 V). The reaction that occurred in the lower voltage region (1.5 V−2.4 V) was less important with regard to capacity decay.

To increase our understanding of the electrochemical process that occurs in $Li_xC_6O_6$, cyclic voltammetry (CV) was conducted at various scan rates from 0.1 to 0.8 mV s^{-1}. Figure 2a shows that two major redox peaks appeared at each scan rate, in agreement with the galvanostatic experiment. Note that the current peaks are linear with respect to the square-root of the scan rates in Figure 2b,c, indicating that the redox reactions in the electrode are bulk diffusion-controlled and not surface-limited.[21,22] While earlier reports discussed the Li storage

dx.doi.org/10.1021/jz501557n | J. Phys. Chem. Lett. 2014, 5, 3086−3092

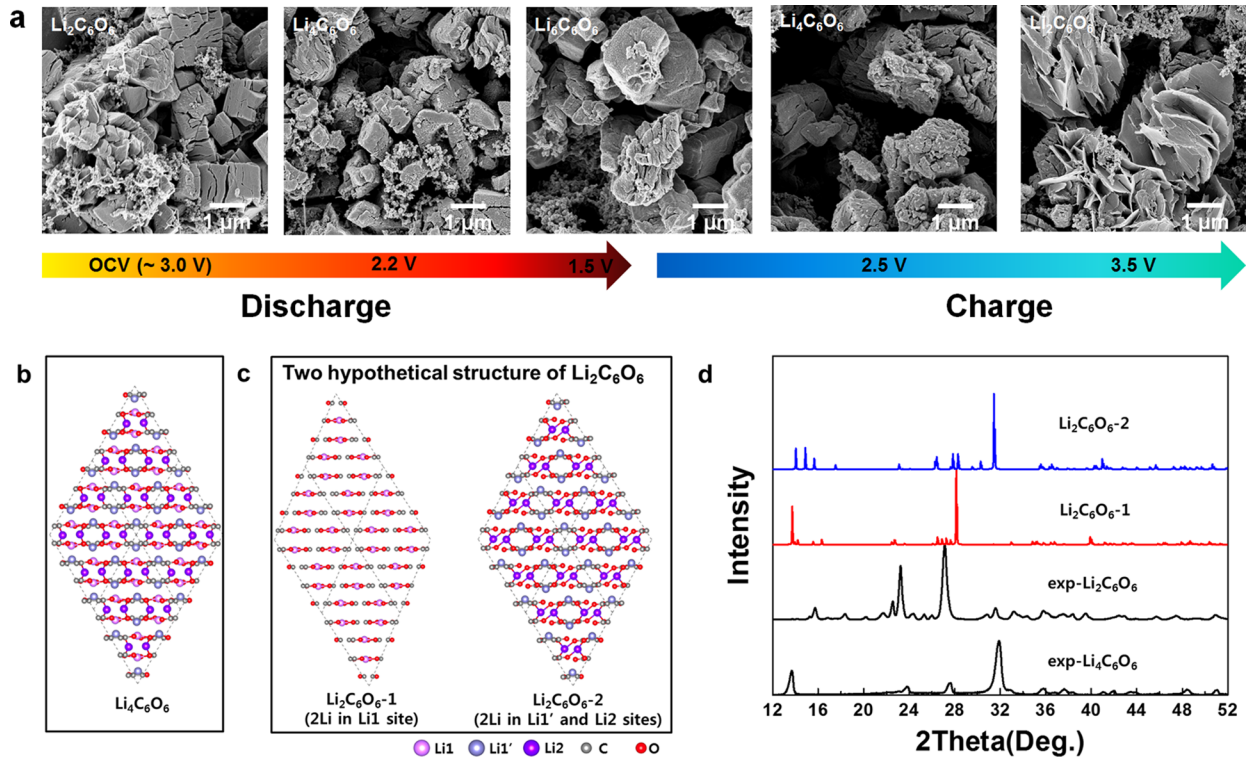

Figure 4. (a) Morphological changes in the $Li_2C_6O_6$ electrode are shown as a result of the charge/discharge process. (b) Crystal structure of $Li_4C_6O_6$. (c) Predicted crystal structures of $Li_2C_6O_6$. The crystal structure of $Li_2C_6O_6$-1 after the extraction of Li ions in the interlayer between C_6O_6 molecules is displayed on the left. The crystal structure of $Li_2C_6O_6$-2 after the extraction of Li ions in the C_6O_6 layers are shown on the right. Purple, gray, and red spheres represent Li, C, and O atoms, respectively. (d) Generated XRD diffractograms of $Li_2C_6O_6$-1 and $Li_2C_6O_6$-2 are presented with analogous experimental data.

mechanism in organic compounds using a one molecule-based picture, whereby Li ions are simply bound to the C═O bond of a molecule,[17,23,24] our results clearly suggested that Li diffusion through the crystal structure and its occupation at interstitial sites provides a realistic mechanism of the electrochemical reaction.[25] Most notable here is that the cathodic peak current (C1) was far less responsive to the scan rates than the anodic peak current response (A1), while the cathodic (C2) and anodic (A2) peak currents showed a similar sensitivity to each other with respect to the scan rates. This behavior indicated that the de/lithiation process is kinetically imbalanced in the region of $Li_xC_6O_6$ ($2 \leq x \leq 4$), which differed from $Li_xC_6O_6$ ($4 \leq x \leq 6$). The QOCP measurement of $Li_xC_6O_6$ in Figure 2d further confirmed that in line with the CV results, the lithiation process exhibited a larger polarization at a given relaxation time than the delithiation process, suggesting that the lithiation kinetics of $Li_2C_6O_6$ is relatively slow compared to the delithiation kinetics of $Li_4C_6O_6$. It is also worth noting that the polarization is generally larger in the region of $2 \leq x \leq 4$ than that of $4 \leq x \leq 6$. Later, this phenomenon will be discussed in detail in the context of the structural changes of the electrode.

Further galvanostatic analyses were conducted with PITT measurements as shown in Figure 2e to determine the nature of the insertion process (one-phase vs two-phase).[26,27] The characteristic shape of the current versus time curve provides useful information regarding the mechanism of the electrochemical reaction.[28] Local maxima can be observed clearly in the upper plateau that follows a bell-shape in Figure 2e. Such a "bell-shaped" curve with a local maximum current for each individual titration is generally indicative of a two-phase nucleation- and growth-based reaction during de/lithiation.[29] This implies that the de/lithiation process in $Li_xC_6O_6$ ($2 \leq x \leq 4$) is likely a two-phase reaction. While the bell-shaped current signature can also be obtained from the heterogeneous charging of a porous electrodes with homogeneous intercalation (switching between single phases) within individual particles, it was noted that the current shape obtained from our PITT analysis is very similar to the current signature of $LiFePO_4$ (a representative material with two-phase behavior) in the literature.[30,31] Also, all the particles are in electric contact with each other in the electrode, indicating the potential applied to all particles should be the same.[32] Thus, the condition of the heterogeneous charging of electrodes is less plausible. Local maxima were not as obvious as for on the lower plateau, although determining if the curve exhibited Cottrell-type behavior was challenging.

To further explore this reaction mechanism, the structural evolution of the $Li_xC_6O_6$ electrode during cycling was monitored at various discharged and charged states using ex situ XRD, as illustrated in Figure 3. Figure 3a shows that a new set of XRD peaks clearly evolved as the $Li_2C_6O_6$ electrode discharged in the upper plateau. The magnified image in Figure 3b shows that the main new peak appears at ~32°, which corresponded with the main XRD peak of $Li_4C_6O_6$ that we synthesized chemically (Figure S3).[15,25] In contrast, no shift in the 27.2° peak from $Li_2C_6O_6$ was observed during the lithiation process. This indicated that the lithiation of $Li_xC_6O_6$ ($2 \leq x \leq 4$) occurred through a two-phase nucleation and growth mechanism between $Li_2C_6O_6$ and $Li_4C_6O_6$, which is in good agreement with electrochemical observations. Further discharge through the lower plateau produced another new XRD peak near 26° with the disappearance of the peak at 32°. Although

dx.doi.org/10.1021/jz501557n | J. Phys. Chem. Lett. 2014, 5, 3086−3092

the peak at 32° could not be indexed due to the lack of structural information on $Li_6C_6O_6$, these results demonstrate that the lithiation of $Li_xC_6O_6$ ($4 \leq x \leq 6$) also occurs via a nucleation and growth mechanism from $Li_4C_6O_6$ and $Li_6C_6O_6$. For the charging process in Figure 3c,d, we observed the opposite phenomenon (i.e., the disappearance of the peak at 26° and concurrent appearance of the peak at 32°), indicating the conversion from $Li_6C_6O_6$ to $Li_4C_6O_6$. In addition, the delithiation of $Li_4C_6O_6$ resulted in disappearance of the XRD peak at 32° and the recovery of the peak at 27°. After complete delithiation, the overall XRD patterns returned to that of the initial stage, except for slight residual peaks of $Li_4C_6O_6$ (in particular, at 14°). The presence of the peak at 14° is believed to be related to the incomplete structural transformation of $Li_4C_6O_6$ during the discharge and charge processes. Very recently, it was revealed that the two-phase based reaction in $LiFePO_4$ can be suppressed above a critical current rate.[33,34] Similar behavior was found in $Li_2C_6O_6$ electrode, where the voltage plateaus become slope at an increased current rate, which is attributable to the suppression of phase separation during battery cycling (Figure S4a). As a result, the cycle performance could be slightly improved (Figure S4b).

The structural stability of $Li_xC_6O_6$ was examined in the presence of the electrolyte using Fourier transform infrared (FT-IR) analyses. While the dissolution of organic electrodes into the organic electrolyte is generally attributable to capacity degradation during cycling,[18,35,36] our test was performed for $Li_2C_6O_6$ and $Li_4C_6O_6$, since the capacity decay mainly occurred in the region of $Li_xC_6O_6$ ($2 \leq x \leq 4$) (Figure S2). FT-IR spectra of $Li_2C_6O_6$, $Li_4C_6O_6$ powders, and the electrolyte were used as references. However, we found that no dissolution of $Li_2C_6O_6$ and $Li_4C_6O_6$ in the electrolyte were noticeable even after storage in the electrolyte for 7 days, as shown in Figure S5, which indicates that both $Li_2C_6O_6$ and $Li_4C_6O_6$ are relatively stable in the electrolyte. The possibility that the dissolved electrode material was deposited on other parts of the cell, such as the separator, was examined using SEM analyses (Figure S6). However, no such deposits were observed, supporting that $Li_xC_6O_6$ ($2 \leq x \leq 4$) did not dissolve in the electrolyte after battery cycling. We further tested the dissolution behavior of $Li_2C_6O_6$ in the electrolyte. The $Li_2C_6O_6$ and $Li_4C_6O_6$ were stored in the electrolyte for 48 h (Figure S7). The color of $Li_2C_6O_6$ in the electrolyte is slightly changed, indicating $Li_2C_6O_6$ can be dissolved in the electrolyte upon battery cycling. To further understand whether the dissolution of the electroactive material in the electrolyte is the major reason for the capacity degradation, we designed a galvanostatic measurement (Figure S8). Although $Li_2C_6O_6$ is cycled with rest time (5 min.) for each cycle to exposure $Li_2C_6O_6$ electrode for electrolyte more time, no noticeable change in capacity performance is observed. This behavior indicates that the dissolution of $Li_2C_6O_6$ could not be the major issue for the capacity degradation although $Li_2C_6O_6$ can be dissolved in the electrolyte. Instead, we observed significant morphological changes for $Li_2C_6O_6$ electrodes using ex situ SEM analyses. Figure 4a shows that, while the morphology of the $Li_2C_6O_6$ electrodes was not significantly altered during discharge, upon the charging process, the electrode particles exhibited notable cracks and were eventually exfoliated. The exfoliation was most prominent when $Li_4C_6O_6$ was electrochemically transformed to $Li_2C_6O_6$. This behavior was not restricted to local regions but occurred throughout the entire electrode (Figure S9). Thus, we believe that the exfoliation of the electrode upon battery cycling can accelerate the dissolution of electroactive material in the electrolyte owing to the increased surface area, which in turn deteriorates capacity stability.

Using first-principles analysis of $Li_xC_6O_6$ during de/lithiation, we attempted to elucidate the particle exfoliation during charging and found that it may be related to changes in the crystal structure of the electrode. While the detailed crystal structure of $Li_2C_6O_6$ remains unknown, we previously predicted that $Li_4C_6O_6$ is composed of a layered structure containing horizontally ordered layers of C_6O_6 molecules with three types of energetically favorable Li sites:[25] (i) the Li1 site, which is located within a layer of C_6O_6 molecules; (ii) the Li1′ site, which is similar to the Li1 site but slightly shifted from the C_6O_6 layers due to electrostatic repulsion from nearby Li ions; and (iii) the Li2 site, which is located between the C_6O_6 layers (Figure 4b). Based on our predicted structure of $Li_4C_6O_6$, we carried out first-principles calculations for $Li_2C_6O_6$, suggesting that Li removal of Li1′ and Li2 sites from the $Li_4C_6O_6$ structure (denoted as $Li_2C_6O_6$-1) is more energetically favorable (by 126 meV) than if two Li ions are extracted from Li1 sites of the $Li_4C_6O_6$ structure (denoted as $Li_2C_6O_6$-2; Figure 4c). Moreover, our predicted XRD pattern based on our hypothetical $Li_2C_6O_6$-1 structure agreed better with that of the experimentally obtained $Li_2C_6O_6$, as illustrated in Figure 4d. There are slight difference in the relative peak intensity and position still noticeable, indicating that more precise structural determination of $Li_2C_6O_6$ would be useful. Specifically, the main peak of $Li_2C_6O_6$-1 (27.8°) was much closer to the experimental value (27.1°) than the peak obtained using $Li_2C_6O_6$-2 (31.5°). Compared to $Li_4C_6O_6$, the primary peak shifted significantly to a lower angle in the case of $Li_2C_6O_6$-1, possibly because Li ions located in the interlayers (i.e., Li2 and Li1′) were removed from the structure, which weakened the binding between C_6O_6 layers. In contrast, no significant shift in the main peak was observed for $Li_2C_6O_6$-2 compared to $Li_4C_6O_6$ because Li ions remained bound to the C_6O_6 layers. The interlayer space expanded from 2.805 to3.169 Å with the extraction of Li ions from $Li_4C_6O_6$ to $Li_2C_6O_6$. We believe that the extraction of Li from C_6O_6 interlayers, as predicted from first-principles calculations, decreases the binding force between the C_6O_6 layers during the conversion from $Li_4C_6O_6$ to $Li_2C_6O_6$, which can lead to a feasible intercalation of large organic molecules into C_6O_6 layers or pulverization at the electrode level (Figure S10). This is in contrast to the electrochemical reaction between $Li_4C_6O_6$ and $Li_6C_6O_6$, where Lis are always present between C_6O_6 layers independent of the state of the charge. Upon repeated battery cycling between $Li_2C_6O_6$ and $Li_4C_6O_6$, a gradual degradation of the microstructure is expected due to the large change in the interslab space. This expectation is consistent with our morphology study in Figure 4a and with very recent studies on organic electrode materials whereby volume expansion and shrinkage during battery operation led to decreased capacity.[19,37,38] Some layered electrode materials are known to be susceptible to exfoliation when the interlayer is empty, since this results in enlarged spacing.[39] As a consequence of these structural variations, pulverization of the electrode is likely to occur, which may cause the electrical isolation of particles and leading subsequently to degradation in the capacity. We expect that material tuning at the molecular level may be able to address this problem, for example, sodium or potassium doping of $Li_xC_6O_6$. This can be done without a significant structural change because of the similarity of the crystal structures

dx.doi.org/10.1021/jz501557n | J. Phys. Chem. Lett. 2014, 5, 3086−3092

between $Li_2C_6O_6$ and $A_2C_6O_6$ (A = Na and K), which all have layered structure.[40,41] Moreover, larger ions such as Na and K occupy the sites between the C_6O_6 layers in their own structures, $Na_2C_6O_6$ and $K_2C_6O_6$. Thus, larger dopant may substitute the Li2 site and aid in binding of the C_6O_6 through the interaction with oxygen atoms even after Li extraction during charging, thus preventing exfoliation. Even though this dopant will take Li sites, thus reduce capacity, but this small amount of doping would decrease the capacity degradation while maintaining the electroactive material.

In summary, herein, the electrochemical reaction mechanism and origin of capacity degradation in $Li_2C_6O_6$ electrodes were verified using electrochemical and ex situ characterization. The dissolution of the active material into the surrounding electrolyte, which is generally believed to be the main cause of capacity decay in most organic electrode materials, was not a sole factor in this material. Instead, exfoliation of C_6O_6 layers resulted in electrode exfoliation and it can accelerate the dissolution of electroactive material in the electrolyte owing to the increased surface area. This behavior results in a degradation of capacity during repeated battery cycling. The susceptibility of exfoliation is attributable to the unique structural changes associated with the sequence of Li ion extraction from this layered material. This work suggests that various factors of both dissolution and of crystal structural stability should be considered when determining causes of capacity decay in such organic electrode materials. Our results provided herein should help the design of optimized electrodes fabricated from electroactive organic materials.

■ ASSOCIATED CONTENT

Supporting Information

Experimental details. Computational details. TGA/DSC, charge/discharge profiles at several voltage cutoff, XRD pattern of $Li_4C_6O_6$, FT-IR spectrum, SEM images of separators after cycling, SEM images of $Li_2C_6O_6$ after discharge, and photographs of the electrodes after battery cycling. This material is available free of charge via the Internet at http://pubs.acs.org.

■ AUTHOR INFORMATION

Corresponding Authors

*E-mail address: leeys@chonnam.ac.kr (Y.S.L.).
*E-mail address: wsyoon@skku.edu (W.-S.Y.).
*E-mail address: matlgen1@snu.ac.kr Tel.: +82-2-880-7088 Fax.: +82-2-885-9671 (K.K.).

Present Address

[#](D.H.S.) Department of Materials Science and Engineering, Massachusetts Institute of Technology, Cambridge, Massachusetts 02139, United States.

Notes

The authors declare no competing financial interest.

■ ACKNOWLEDGMENTS

This work was supported by (i) the Supercomputing Center/Korea Institute of Science and Technology Information with supercomputing resources including technical support (KSC-2012-C3-049) and (ii) the Human Resources Development program (20124010203320) of the Korea Institute of Energy Technology Evaluation and Planning (KETEP) grant funded by the Korea government Ministry of Trade, Industry and Energy. This work was also supported by (iii) the National Research Foundation of Korea Grant funded by the Korean Government (MEST) (NRF-2009-0094219) and (iv) the Energy Efficiency & Resources of the Korea Institute of Energy Technology Evaluation and Planning (KETEP) grant funded by the Korea government Ministry of Trade, Industry & Energy (MOTIE) (No.20132020000270).

■ REFERENCES

(1) Tarascon, J. M.; Armand, M. Issues and Challenges Facing Rechargeable Lithium Batteries. *Nature* **2001**, *414*, 359−367.
(2) Kang, K.; Meng, Y. S.; Bréger, J.; Grey, C. P.; Ceder, G. Electrodes with High Power and High Capacity for Rechargeable Lithium Batteries. *Science* **2006**, *311*, 977−980.
(3) Poizot, P.; Laruelle, S.; Grugeon, S.; Dupont, L.; Tarascon, J. M. Nano-Sized Transition-Metal Oxides as Negative-Electrode Materials for Lithium-Ion Batteries. *Nature* **2000**, *407*, 496−499.
(4) Lee, J.; Urban, A.; Li, X.; Su, D.; Hautier, G.; Ceder, G. Unlocking the Potential of Cation-Disordered Oxides for Rechargeable Lithium Batteries. *Science* **2014**, *343*, 519−522.
(5) Kim, H.; Lim, H.-D.; Kim, S.-W.; Hong, J.; Seo, D.-H.; Kim, D.-c.; Jeon, S.; Park, S.; Kang, K. Scalable Functionalized Graphene Nanoplatelets as Tunable Cathodes for High-Performance Lithium Rechargeable Batteries. *Sci. Rep.* **2013**, *3*, 1506.
(6) McDowell, M. T.; Lee, S. W.; Ryu, I.; Wu, H.; Nix, W. D.; Choi, J. W.; Cui, Y. Novel Size and Surface Oxide Effects in Silicon Nanowires as Lithium Battery Anodes. *Nano Lett.* **2011**, *11*, 4018−4025.
(7) Hy, S.; Felix, F.; Rick, J.; Su, W.-N.; Hwang, B. J. Direct In situ Observation of Li_2O Evolution on Li-Rich High-Capacity Cathode Material, $Li[Ni_xLi_{(1-2x)/3}Mn_{(2-x)/3}]O_2$ ($0 \le x \le 0.5$). *J. Am. Chem. Soc.* **2013**, *136*, 999−1007.
(8) Jung, Y. S.; Lu, P.; Cavanagh, A. S.; Ban, C.; Kim, G.-H.; Lee, S.-H.; George, S. M.; Harris, S. J.; Dillon, A. C. Unexpected Improved Performance of ALD Coated $LiCoO_2$/Graphite Li-Ion Batteries. *Adv. Energy Mater.* **2013**, *3*, 213−219.
(9) Mizushima, K.; Jones, P. C.; Wiseman, P. J.; Goodenough, J. B. Li_xCoO_2 ($0 < x < 1$): A New Cathode Material for Batteries of High Energy Density. *Mater. Res. Bull.* **1980**, *15*, 783−789.
(10) Yamada, A.; Chung, S. C.; Hinokuma, K. Optimized $LiFePO_4$ for Lithium Battery Cathodes. *J. Electrochem. Soc.* **2001**, *148*, A224−A229.
(11) Tarascon, J.-M. Towards Sustainable and Renewable Systems for Electrochemical Energy Storage. *ChemSusChem* **2008**, *1*, 777−779.
(12) Yang, P.; Tarascon, J.-M. Towards Systems Materials Engineering. *Nat. Mater.* **2012**, *11*, 560−563.
(13) Armand, M.; Grugeon, S.; Vezin, H.; Laruelle, S.; Ribiere, P.; Poizot, P.; Tarascon, J. M. Conjugated Dicarboxylate Anodes for Li-Ion Batteries. *Nat. Mater.* **2009**, *8*, 120−125.
(14) Chen, H.; Armand, M.; Demailly, G.; Dolhem, F.; Poizot, P.; Tarascon, J.-M. From Biomass to a Renewable $Li_xC_6O_6$ Organic Electrode for Sustainable Li-Ion Batteries. *ChemSusChem* **2008**, *1*, 348−355.
(15) Chen, H.; Armand, M.; Courty, M.; Jiang, M.; Grey, C. P.; Dolhem, F.; Tarascon, J.-M.; Poizot, P. Lithium Salt of Tetrahydroxybenzoquinone: Toward the Development of a Sustainable Li-Ion Battery. *J. Am. Chem. Soc.* **2009**, *131*, 8984−8988.
(16) Novák, P.; Müller, K.; Santhanam, K.; Haas, O. Electrochemically Active Polymers for Rechargeable Batteries. *Chem. Rev.* **1997**, *97*, 207−282.
(17) Han, X.; Chang, C.; Yuan, L.; Sun, T.; Sun, J. Aromatic Carbonyl Derivative Polymers as High-Performance Li-Ion Storage Materials. *Adv. Mater.* **2007**, *19*, 1616−1621.
(18) Liang, Y.; Tao, Z.; Chen, J. Organic Electrode Materials for Rechargeable Lithium Batteries. *Adv. Energy Mater.* **2012**, *2*, 742−769.
(19) Liang, Y.; Zhang, P.; Yang, S.; Tao, Z.; Chen, J. Fused Heteroaromatic Organic Compounds for High-Power Electrodes of Rechargeable Lithium Batteries. *Adv. Energy Mater.* **2013**, *3*, 600−605.

(20) Liang, Y.; Zhang, P.; Chen, J. Function-Oriented Design of Conjugated Carbonyl Compound Electrodes for High Energy Lithium Batteries. *Chem. Sci.* **2013**, *4*, 1330−1337.
(21) Pournaghi-Azar, M. H.; Sabzi, R. Electrochemical Characteristics of a Cobalt Pentacyanonitrosylferrate Film on a Modified Glassy Carbon Electrode and Its Catalytic Effect on the Electrooxidation of Hydrazine. *J. Electroanal. Chem.* **2003**, *543*, 115−125.
(22) Julien, C.; Haro-Poniatowski, E.; Camacho-Lopez, M. A.; Escobar-Alarcon, L.; Jimenez-Jarquin, J. Growth of $LiMn_2O_4$ Thin Films by Pulsed-Laser Deposition and Their Electrochemical Properties in Lithium Microbatteries. *Mater. Sci. Eng.: B* **2000**, *72*, 36−46.
(23) Le Gall, T.; Reiman, K. H.; Grossel, M. C.; Owen, J. R. Poly(2,5-dihydroxy-1,4-benzoquinone-3,6-methylene): A New Organic Polymer as Positive Electrode Material for Rechargeable Lithium Batteries. *J. Power Sources* **2003**, *119−121*, 316−320.
(24) Zeng, R.-h.; Li, X.-p.; Qiu, Y.-c.; Li, W.-s.; Yi, J.; Lu, D.-s.; Tan, C.-l.; Xu, M.-q. Synthesis and Properties of a Lithium-Organic Coordination Compound as Lithium-Inserted Material for Lithium Ion Batteries. *Electrochem. Commun.* **2010**, *12*, 1253−1256.
(25) Seo, D.-H.; Kim, H.; Kim, H.; Goddard, W. A.; Kang, K. The Predicted Crystal Structure of $Li_4C_6O_6$, an Organic Cathode Material for Li-Ion Batteries, from First-Principles Multi-Level Computational Methods. *Energy & Environ. Sci.* **2011**, *4*, 4938−4941.
(26) Park, Y.; Shakoor, R.; Park, K. Y.; Kang, K. Charge/Discharge Mechanism of Multicomponent Olivine Cathode for Lithium Rechargeable Batteries. *J. Electrochem. Sci. Technol.* **2011**, *2*, 14−19.
(27) Meethong, N.; Huang, H. Y. S.; Speakman, S. A.; Carter, W. C.; Chiang, Y. M. Strain Accommodation during Phase Transformations in Olivine-Based Cathodes as a Materials Selection Criterion for High-Power Rechargeable Batteries. *Adv. Funct. Mater.* **2007**, *17*, 1115−1123.
(28) Nishina, T.; Ura, H.; Uchida, I. Determination of Chemical Diffusion Coefficients in Metal Hydride Particles with a Microelectrode Technique. *J. Electrochem. Soc.* **1997**, *144*, 1273−1277.
(29) Meethong, N.; Kao, Y.-H.; Speakman, S. A.; Chiang, Y.-M. Aliovalent Substitutions in Olivine Lithium Iron Phosphate and Impact on Structure and Properties. *Adv. Funct. Mater.* **2009**, *19*, 1060−1070.
(30) Levi, M. D.; Sigalov, S.; Salitra, G.; Nayak, P.; Aurbach, D.; Daikhin, L.; Perre, E.; Presser, V. Collective Phase Transition Dynamics in Microarray Composite Li_xFePO_4 Electrodes Tracked by in Situ Electrochemical Quartz Crystal Admittance. *J. Phys. Chem. C* **2013**, *117*, 15505−15514.
(31) Bai, P.; Bazant, M. Z. Charge Transfer Kinetics at the Solid−Solid Interface in Porous Electrodes. *Nat. Commun.* **2014**, *5*, 3585.
(32) Madej, E.; La Mantia, F.; Schuhmann, W.; Ventosa, E. Impact of the Specific Surface Area on the Memory Effect in Li-Ion Batteries: The Case of Anatase TiO_2. *Adv. Energy Mater.* **2014**, DOI: 10.1002/aenm.201400829.
(33) Zhang, X.; van Hulzen, M.; Singh, D. P.; Brownrigg, A.; Wright, J. P.; van Dijk, N. H.; Wagemaker, M. Rate-Induced Solubility and Suppression of the First-Order Phase Transition in Olivine $LiFePO_4$. *Nano Lett.* **2014**, *14*, 2279−2285.
(34) Niu, J.; Kushima, A.; Qian, X.; Qi, L.; Xiang, K.; Chiang, Y.-M.; Li, J. In Situ Observation of Random Solid Solution Zone in $LiFePO_4$ Electrode. *Nano Lett.* **2014**, *14*, 4005−4010.
(35) Lee, M.; Hong, J.; Kim, H.; Lim, H.-D.; Cho, S. B.; Kang, K.; Park, C. B. Organic Nanohybrids for Fast and Sustainable Energy Storage. *Adv. Mater.* **2014**, *26*, 2558−2565.
(36) Lee, M.; Hong, J.; Seo, D.-H.; Nam, D. H.; Nam, K. T.; Kang, K.; Park, C. B. Redox Cofactor from Biological Energy Transduction as Molecularly Tunable Energy-Storage Compound. *Angew. Chem., Int. Ed.* **2013**, *52*, 8322−8328.
(37) Luo, C.; Huang, R.; Kevorkyants, R.; Pavanello, M.; He, H.; Wang, C. Self-Assembled Organic Nanowires for High Power Density Lithium Ion Batteries. *Nano Lett.* **2014**, *14*, 1596−1602.
(38) Luo, C.; Zhu, Y.; Xu, Y.; Liu, Y.; Gao, T.; Wang, J.; Wang, C. Graphene Oxide Wrapped Croconic Acid Disodium Salt for Sodium Ion Battery Electrodes. *J. Power Sources* **2014**, *250*, 372−378.
(39) Oh, E.-J.; Kim, T. W.; Lee, K. M.; Song, M.-S.; Jee, A.-Y.; Lim, S. T.; Ha, H.-W.; Lee, M.; Choy, J.-H.; Hwang, S.-J. Unilamellar Nanosheet of Layered Manganese Cobalt Nickel Oxide and Its Heterolayered Film with Polycations. *ACS Nano* **2010**, *4*, 4437−4444.
(40) Dinnebier, R. E.; Nuss, H.; Jansen, M. Disodium Rhodizonate: A Powder Diffraction Study. *Acta Crystallogr., Sect. E* **2005**, *61*, m2148−m2150.
(41) Cowan, J. A.; Howard, J. A. K. Dipotassium Rhodizonate. *Acta Crystallogr., Sect. E* **2004**, *60*, m511−m513.